AIAA JOURNAL
Vol. 31, No. 9, September 1993

Flow and Heat Transfer in a Turbulent Boundary Layer Through Skewed and Pitched Jets

Xin Zhang* and Michael W. Collins†
City University, London EC1V 0HB, England, United Kingdom

A study was carried out of longitudinal vortices in a low speed turbulent boundary layer due to small jets. The jet was pitched at 45 deg and skewed between 0 and 120 deg. The effects of jet velocity ratio ($0 \le \lambda_j \le 3.0$) and skew angle ($0 \le \theta \le 120$ deg) were addressed. Mass-averaged Navier-Stokes equations were solved using computational fluid dynamics and heat transfer. Turbulence closure was achieved using k-ϵ model. Three types of vortex production were noted at various jet velocity ratios. When a longitudinal vortex is positioned at the edge or in the outer region of the boundary layer, optimal effects of the flow and heat transfer control were achieved. When the vortex lay deeply in the boundary layer, the effects on heat transfer control could be detrimental. When the jet penetrated the boundary layer, the favorable effects of the vortex on control were reduced due to the larger distance away from the surface. Significant improvements of vortex strength and heat transfer were seen between skew angle $0 \le \theta \le 45$ deg, although in $45 < \theta < 120$ deg the improvements were marginal.

Nomenclature

C_{fx}	= longitudinal skin friction coefficient
C_{fz}	= lateral skin friction coefficient
C_p	= specific heat
D	= jet diameter
h	= heat transfer coefficient, $q/(T_s - T_f)$
k	= turbulent kinetic energy
$\underline{Nu}$	= Nusselt number, $h \cdot D/\lambda$
$\overline{Nu}$	= averaged Nusselt number, $1/S\int_s Nu \cdot dx\, dz$
q	= heat flux on the wall, W/m^2
S	= surface area
T	= temperature
T_f	= cross-stream temperature
T_j	= jet exit temperature
T_s	= wall temperature
U, V, W	= velocity components
V	= flow velocity in vector form
V_e	= cross-stream velocity
V_j	= jet exit velocity
x, y, z	= Cartesian coordinates
α	= jet pitch angle
δ	= oncoming boundary-layer thickness
ϵ	= turbulence dissipation rate
ζ	= bulk viscosity
θ	= jet skew angle
λ	= thermal conductivity of air
λ_j	= jet velocity ratio, V_j/V_e
μ	= viscosity
ρ	= density
σ_t	= turbulent Prandtl number
τ	= shear stress
$\bar{\Omega}_x$	= vorticity level on x plane, $\delta/V_e[(\partial W/\partial y)/ - (\partial V/\partial z)]$

I. Introduction

THE fluid flow and thermal fields created by the interaction between a longitudinal vortex and a boundary layer are important in both fundamental research and practical applications. Longitudinal vortices can be produced by an obstruction protruding and a jet exhausting from a wall. There may also be Taylor-Görtler type vortices along a curved surface. Under certain flow and geometric conditions, longitudinal vortices could remain coherent for a long distance, thus exerting influence over a large area. The effects could be either beneficial or detrimental. One of the possible applications of the longitudinal vortices is control of flow and heat transfer. They could, for example, be used for heat transfer enhancement. Convective heat transfer enhancement in both laminar and turbulent flows is a problem of significant engineering importance. The need exists generally in mechanical engineering, and more specifically in gas cooled nuclear reactors, heat exchangers, and turbomachinery. This enhancement should be viewed in the context of CHEX, the compact heat exchanger, that is, that compactness is the desirable design requirement. Such compactness, together with mass reduction, is also required for heat exchangers in aerospace industry. The present study investigates a rarely explored form of flow and heat transfer control—that produced by longitudinal vortices in a turbulent boundary layer through pitched and skewed small jets. (Air jets are used in this study. The results and likely applications, though, should be applicable to fluid jets as well.) A flow and heat transfer model is set up to investigate mass and thermal convection using computational fluid dynamics and heat transfer.

Conventional forms of longitudinal vortex used for flow control are normally produced by small delta and half winglets which are positioned at an angle to an oncoming cross stream. When a winglet is placed in a boundary layer and its size is of the same order as the boundary-layer thickness, a longitudinal vortex forms downstream in or just above the edge of the boundary layer.[1] The winglet is thus called a vortex generator. In practice, arrays of them are usually used in contra- or corotating fashions to delay or even suppress impending separation. They can also be used to promote diffusion in diffuser intakes.[2] Other applications include noise control, combustion promotion, and mixing enhancement in chemical engineering. In addition to the winglet vortex generators, small skewed and pitched jets can also produce longitudinal vortices.[3-8] Although the vortices produced by the jets possess a number of similar features as those due to the winglets, there are some notable differences[5,8] in turbulent flow characteristics and velocity of the vortex core, for example. The flow characteristics and vortex production mechanism are only recently beginning to be understood.

In the middle 1970s, attempts were made to use winglet vortex generators to enhance heat transfer in laminar flow. It was realized that, with an exchange of kinetic energy, thermal

Received June 29, 1992; revision received Nov. 28, 1992; accepted for publication Dec. 1, 1992.

*Lecturer, Department of Mechanical Engineering and Aeronautics. Member AIAA.

†Professor, Department of Mechanical Engineering and Aeronautics.

energy was also exchanged. Edwards and Alker[9] used three-dimensional surface protrusions to generate longitudinal vortices, which included cubes and small winglets. The cubes were found to produce the highest local improvement, but the effect of the winglets extended farther downstream. Of the winglet vortex generators, the contrarotating systems were the more effective. Later, applications were found for plate-fin and fin-tube surface heat transfer enhancement.[10-12] These researches generally dealt with laminar flows and were aimed at specific applications. The emphasis on application-related studies probably reflects a general lack of understanding of basic flow mechanism and the restriction to laminar cases shows the development requirements by industries so far. There are, though, increasingly bigger requirements for better understanding of vortex generator flows in general, and turbulent vortex generator flows in the aerospace industry in particular. A model of flow and heat transfer mechanism must be established before engineering applications become a reality.

Eibeck and Eaton[13] carried out an experimental study of heat transfer characteristics of a longitudinal vortex in turbulent flow using a winglet and a turbulent boundary layer. They suggested that the dominant mechanism was two dimensional, and that the vortex modified the local behavior through the process of convecting kinetic and thermal energy within the boundary layer. This assessment remains to be clarified through further study. The mass and thermal field could be affected through changes in the two-dimensional mean flowfield as well as by turbulent diffusion due to the vortex. It could be argued that since the vortex strength is controlled by the turbulent diffusion after an initial stage, the capability of mass convection is affected as well. Although studies of the thermal field are rare, there have been some studies of the fluid flowfield. Opinions of the flow control mechanism range from thinning of the boundary layer to mass convection by the vortex. To understand these mechanisms, a coupled study of fluid flow and thermal fields is needed.

Winglet vortex generators, though, have certain limitations associated with them. They are designed for one particular flow situation and are very much passive devices. Once in place, they cannot be easily moved. When not needed, they may induce some unwanted side effects. For example, they could cause parasite drag during aircraft cruise and hot spots on aerodynamic surfaces and heat exchanger walls. These limitations can be avoided by the use of air jets. Such jets can be used in an integral design process and actively for flow and heat transfer control. The setting of the jets can be changed to suit various flow conditions. It has been proven that the strength of the jet does not need to be exceedingly high for a strong vortex to form.[4,5,8] This effectively removes the requirement for complex jet production systems in the flow control applications.

In this study, the longitudinal vortices generated by a small pitched and skewed jet in a turbulent boundary layer are utilized to investigate flow and convective heat transfer mechanisms. Both turbulent fluid flow and thermal fields are considered. The effects studied include jet velocity ratio and skew angle. The results should be relevant to the winglet vortex generators and longitudinal vortices in laminar flows as well.

II. Flow Conditions

A schematic of the coordinate system and flow domain is shown in Fig. 1. The coordinate system is not a right-hand one. The flow is incompressible and turbulent. Air density, for both cross stream and jet, is 1.225 kg/m^3 and molecular viscosity is 1.789×10^{-5} kg/ms. A fully developed flat-plate turbulent boundary layer is used. The oncoming boundary layer has a thickness δ of 14 mm and the Reynolds number based on its momentum thickness is 1800. A small turbulent jet is generated from a circular orifice (of diameter $D = 6.35$ mm), on the flat plate into the cross stream. The cross-stream temperature T_f is given as 311.15 K and the surface temperature T_s as 305 K at the inlet of the flow domain (see Sec. III.B on boundary conditions). The air jet temperature T_j is the same as that of the cross stream. A constant heat flux rate of -500 W/m^2 is applied on the surface. The oncoming flow speed V_e is fixed at 15 m/s; the jet velocity V_j ranges from $0.25V_e$ to $3.0\ V_e$; the pitch angle α is fixed at 45 deg; and the skew angle θ varies from 0 to 120 deg. The flow and thermal conditions are selected to facilitate comparisons with published experimental data[5] and future experiments planned to be carried out in a comparable wind tunnel.

Results are presented in the forms of velocity vector, skin friction coefficient, nondimensional vorticity level, Nusselt number, and an average Nusselt number defined over an area which covers $-6D$ to $59D$ in the longitudinal direction and $-5D$ to $5D$ in the lateral direction. The jet center is defined as the maximum vorticity point. This definition is justified as the present analysis shows that the main longitudinal vortex closely follows the jet, and the high turbulent kinetic energy core which is sometimes used to define the jet is caused by the fluid swept away by the vortex.

III. Numerical Model

A. Governing Equations

The basic equations used to describe the flow and heat transfer comprise equations for conservation of mass, momentum, and energy. Turbulence is simulated by a standard k-ϵ model.[14] The governing equations in vector form can be written as

$$\frac{\partial \rho}{\partial t} + \nabla \cdot (\rho V) = 0 \tag{1}$$

$$\frac{\partial \rho V}{\partial t} + \nabla \cdot (\rho V \otimes V) - \nabla \cdot (\mu \nabla V) = \nabla [p + \tfrac{2}{3}\rho k + (\tfrac{2}{3}\mu - \zeta)\nabla \cdot V] + \nabla \cdot [\mu (\nabla V)^T] \tag{2}$$

and

$$\frac{\partial \rho T}{\partial t} + \nabla \cdot (\rho V T) - \nabla \cdot \left[\left(\frac{\mu_t}{\sigma_t} + \frac{\lambda}{C_p} \right) \nabla T \right] = 0 \tag{3}$$

where the tensor product is defined as $(A \otimes B)_{ij} = A_i B_j$. The effective viscosity μ is defined by

$$\mu = \mu_l + \mu_t$$

where μ_l is the molecular viscosity and μ_t is the turbulent viscosity.

In the k-ϵ model, μ_t is given as

$$\mu_t = C_\mu \rho (k^2/\epsilon) \tag{4}$$

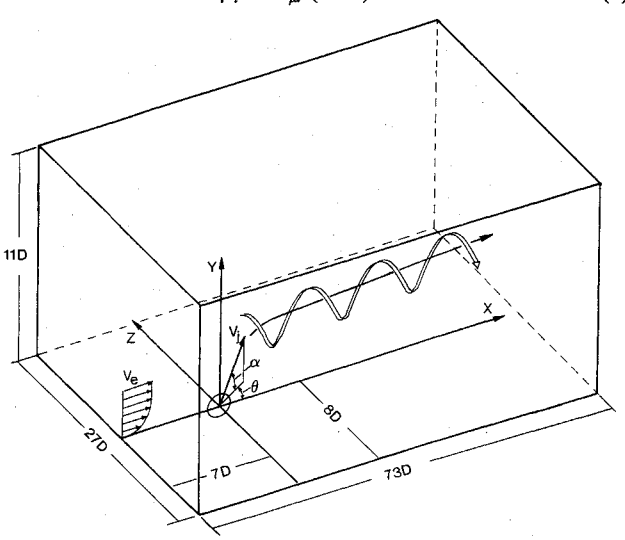

Fig. 1 Schematic of flow and coordinate system.

The transport equations for the turbulent kinetic energy k and the turbulent dissipation rate ϵ are

$$\frac{\partial \rho k}{\partial t} + \nabla \cdot (\rho V k) - \nabla \cdot \left[\left(\mu + \frac{\mu_t}{\sigma_k} \right) \nabla k \right] = P - \rho \epsilon \quad (5)$$

and

$$\frac{\partial \rho \epsilon}{\partial t} + \nabla \cdot (\rho V \epsilon) - \nabla \cdot \left[\left(\mu + \frac{\mu_t}{\sigma_\epsilon} \right) \nabla \epsilon \right] = C_1 \frac{\epsilon}{k} P - C_2 \rho \frac{\epsilon^2}{k} \quad (6)$$

where C_μ, C_1, C_2, σ_k, and σ_ϵ are empirical constants and are given values of 0.09, 1.44, 1.92, 1.0, and 1.3, respectively. P is the shear stress production defined by

$$P = \mu \nabla V \cdot [\nabla V + (\nabla V)^T] - \tfrac{2}{3} \nabla \cdot V (\mu \nabla \cdot V + \rho k) \quad (7)$$

The flow involved consists of areas of swirling and large curvature changes. It is generally realized that the k-ϵ model faces certain difficulties in producing these features. Investigations of longitudinal vortex production using air jets did identify areas of complex turbulent kinetic energy and stress distributions,[8,15] as indeed did an experimental study of winglet vortex generator by Shizawa and Eaton.[16] However, it has also been shown that the most complex turbulent features exist at an early stage of the vortex production. This stage only lasts for a short distance. After it, the vortex development appears to be dominated by a diffusion process through turbulent mixing. The turbulent kinetic energy field and the main stress ($-\overline{u'v'}$) field show largely common features. More importantly, the study demonstrated that the overall flow characteristics, such as the circulation, the maximum vorticity, and the skin friction, could be predicted just as well by the k-ϵ turbulence model and the differential Reynolds stress model. The use of the k-ϵ model in this study is thus believed to be justified.

B. Numerical Approach

In the coordinate system (Fig. 1), the x axis is the longitudinal direction, the y axis the upward direction normal to the flat plate, and the z axis the lateral direction. The physical space in the flow is rectangular, its size varying according to the grid used. A typical grid covers $-8D$ to $65D$, 0–$11D$, and $-8D$ to $19D$ in the x, y, and z directions, respectively. The center of the jet exit is located at the origin of the coordinate system. In the lateral direction where the jet has a positive component, the space covered is extended. For most of the study, a $50 \times 28 \times 42$ grid is used. At least 16 cells are located in the jet exit plane. Around the jet exit, the grid is nonorthogonal in the x-z plane so that the jet exit geometry is modeled correctly. The grid cell size increases gradually in the streamwise and lateral directions. An exponential grid distribution is applied in the y direction and care is taken to locate at least 15 grid points in the boundary layer.

A fully developed velocity profile is used at the inlet and is fixed throughout the computation. The boundary-layer profile is obtained by calculating a two-dimensional turbulent boundary-layer development on a flat plate with an input velocity profile based on the 1/7th law. Initial turbulence data are calculated using an eddy-viscosity model. The initial temperature profile at the inlet is calculated using the Reynolds analogy.

On the outer boundary, derivatives of the variables normal to the boundary are set to zero. Velocity components normal to the boundary are adjusted for mass conservation. On the flat plate, the nonslip condition is used. In the near-wall region, velocity and temperature are calculated using the classic linear-logarithmic wall functions. The heat flux rate on the wall is fixed. On the jet exit surface, the jet velocity is specified. The turbulent kinetic energy k is approximated as

$$k_j = 0.002 V_j^2 \quad (8)$$

and the dissipation rate ϵ as

$$\epsilon_j = k_j^{1.5} / 0.3D \quad (9)$$

The two side boundaries and the top boundary are set as pressure boundaries where the local pressure is fixed as zero. Tests carried out indicate that the pressure boundary and symmetric boundary conditions set on the two lateral sides produce the same results for most parts of the flow. Only when the flow approaches the downstream outlet does the top pressure boundary induce an increase in the skin friction. The results are subsequently not used.

The governing equations are solved using a finite volume solver, FLOW3D. All the terms in the governing equations are discretized in space using second-order central differencing apart from the advective terms and the convection coefficients obtained by the Rhie-Chow interpolation formula.[17] Hybrid differencing is used to treat the advective terms. The SIMPLEC algorithm[18] alternative is used in this work for the pressure-correction equation. The conjugate gradient algorithm is used for the pressure equation, whereas Stone's strongly implicit procedure is used for the other equations. Under-relaxation is used as follows: factors are 0.7 for velocity and 0.4 for k and ϵ. The energy equation is solved separately. The calculation was carried out on a SUN sparc2 station. CPU time and number of iterations vary according to the size of the problem. Convergence is judged to have been achieved when the mass residual is reduced by at least five orders of magnitude.

C. Validation

The present calculation is validated through comparison with predictions using a differential Reynolds stress model[8,15] and with an experimental study.[5] Compton and Johnston's wind-tunnel study[5] provides the only comparable data to the present calculation. They measured velocity distributions at four locations (x = 13, 44, 89, and 135 cm). The present study focuses on the near-field development of the vortex and the flow domain includes only the first measurement plane at x = 13 cm. In Ref. 5 positive circulation and maximum vorticity are given. The measurement is carried out on a 0.5×0.5 cm grid. The positive circulation level for a jet of $\alpha = 45$ deg, $\theta = 45$ deg, and $\lambda_j = 1$ at $x = 13$ cm is 0.026. This compares with the predicted value of 0.0289, which is about 11% higher. Various factors might have contributed to the discrepancy. Among them are the streamwise pressure gradient in the wind tunnel, which is not considered here, and the jet exit geometry, which may alter the induced flow near the exit.[6] As the predicted circulation level varies almost linearly after $X = 40D$, the positive circulation level at $x = 44$ cm is calculated through extrapolation from $x = 41$ cm. The predicted value of $x = 44$ cm is 0.0204. The agreement with the measured value of 0.019 is much better. This observation also applies to the study using a Reynolds stress model where the predicted circulation level converges to the value predicted by the k-ϵ model downstream of the jet exit.

IV. Results and Discussion

A. Jet Induced Vorticity and Stress Fields

The influence of longitudinal vortices in a turbulent boundary layer could be either beneficial or detrimental. The jet needs to be properly set up for a particular flow to enhance the former and mitigate the latter. For flow control, the objective is to create vortices with sufficient strength. For heat transfer enhancement, the task is to promote areas of high heat transfer coefficient and to reduce areas where it is low. Before the correct guidelines can be set, the vortex production mechanism and turbulent stress field should be investigated.

In this study, longitudinal vortex production in a turbulent boundary layer using an unskewed jet ($\alpha = 45$ deg, $\theta = 0$ deg) and a skewed jet ($\alpha = 45$ deg, $\theta = 45$ deg) is investigated. When the jet is unskewed at a pitch angle of $\alpha = 45$ deg, two

contrarotating vortices are produced, and when the jet is skewed, only one stronger vortex is eventually formed.

The production of the contrarotating vortices has been studied extensively in normal jet/cross-stream interaction, which has wide applications in areas such as V/STOL aircraft and missile control. The studies in this area typically set out to investigate a circular jet exhausting normally from a flat plate into a uniform cross stream. The jet trajectory and the induced pressure field have been studied extensively as they are of practical significance in determining the aerodynamic characteristics. The jet surface is usually treated as a vortex sheet represented by a system of longitudinal and ring vortex filaments.[19] The strength of the vortex sheet can be determined by the potential flow theory.[20] The interaction between the oncoming flow and the vortex sheets results in the rolling up of the vortex sheet, and finally, when the jet bends to the cross stream these rolling-up structures form the longitudinal vortices.

If a jet exhausts from a plate into a boundary layer at a pitch angle without skew, the mechanism of forming two contrarotating vortices is basically similar to that described previously. The difference lies in the diffusion process of the vortices. In Fig. 2, velocity vectors on three downstream cross planes are presented for a $\lambda_j = 1.0$ unskewed jet at a pitch angle of $\alpha = 45$ deg. The two contrarotating vortices are clearly visible. Because of the normal velocity of the jet and the induced velocity of the image vortices, the two vortices move away from the wall as they are convected downstream. The surface stress distribution changes. The characteristic stress distributions are given for this flow in Figs. 3a and 3b. The longitudinal skin friction coefficient distribution shows two peaks and a trough. The high skin friction is associated with the high kinetic energy fluid swept to the near wall area and the low skin friction is caused by the stagnant fluid on one side of the vortex. In Fig. 3a, the lateral skin friction coefficient changes sign as the two vortices are contrarotative.

As the jet skews, the vortex production is altered. Subsequently, the mass and thermal convection across the boundary layer are altered as well. Although the initial vorticity production around the jet exit results in vorticity distributions of different signs and two contrarotating vortices of different strengths, the lateral movement of the stronger vortex would engulf the weaker one and eventually form a single vortex. The process is shown by Fig. 4 where a $\lambda_j = 1.0$ jet is skewed at 30 deg and pitched at 45 deg.

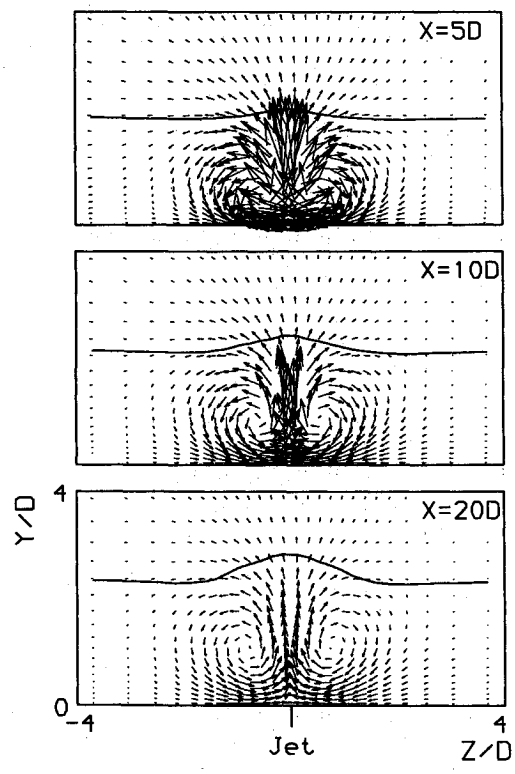

Fig. 2 Velocity vector plots on three downstream cross planes produced by a $\theta = 0$-deg jet: solid line represents the edge of the boundary layer.

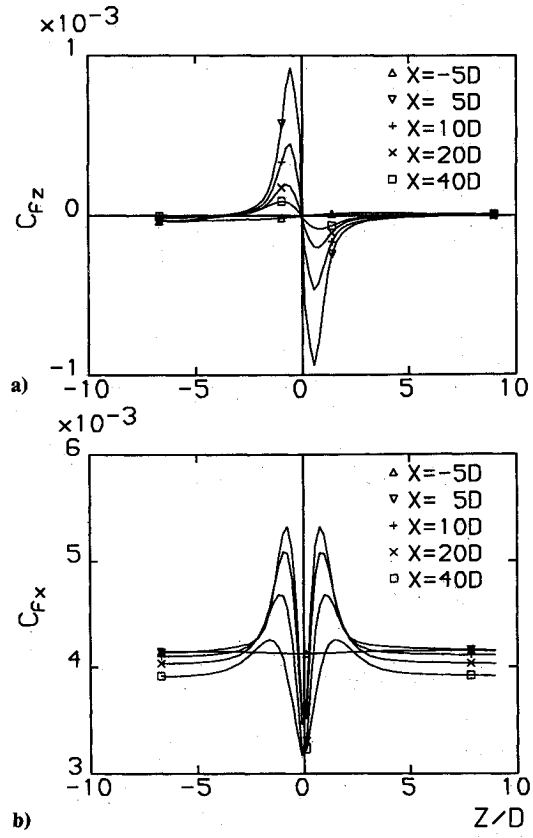

Fig. 3 Stress distribution on the wall produced by a $\theta = 0$-deg jet: a) $C_{fz} = \tau_z/q_e$ and b) $C_{fx} = \tau_x/q_e$.

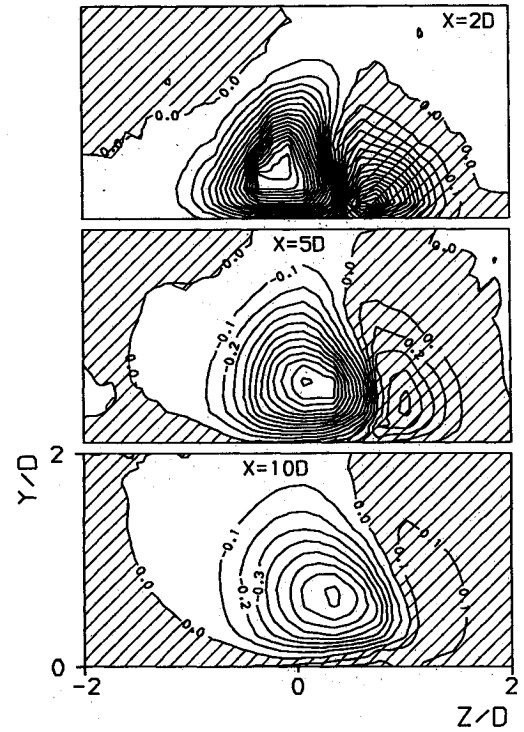

Fig. 4 $\tilde{\Omega}_x$ at three downstream locations due to a $\theta = 30$-deg jet: shaded area indicates induced vorticity.

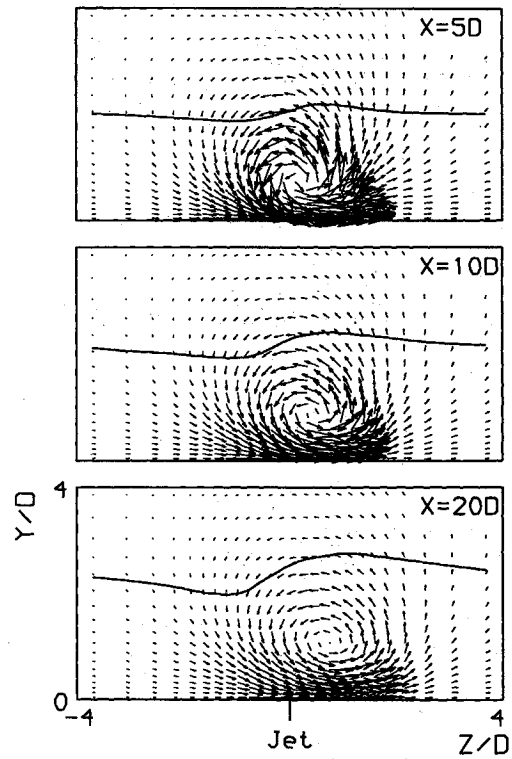

Fig. 5 Velocity vector plots on three downstream cross planes produced by a $\theta = 45$-deg jet: solid line represents the edge of the boundary layer.

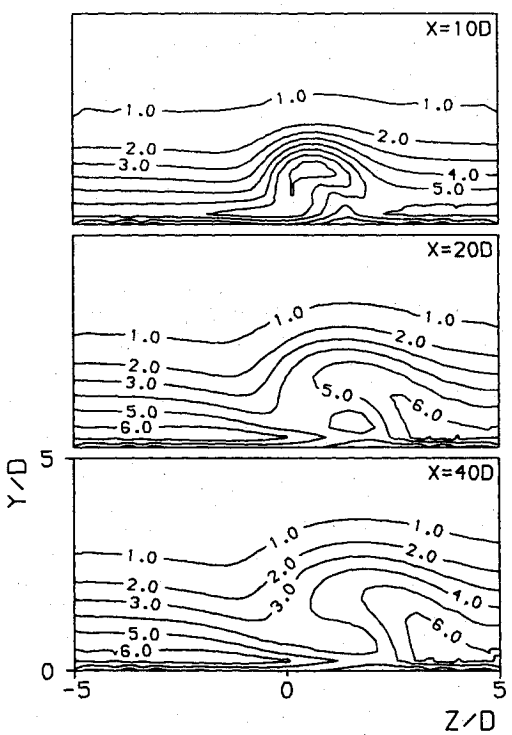

Fig. 6 Turbulent kinetic energy ($k/V_e^2 \cdot 10^3$) distribution downstream of the jet exit produced by a $\theta = 45$-deg and $\lambda_j = 1$ jet.

The secondary vortex (positive vorticity) is quickly engulfed by the main vortex. The main vortex moves in the lateral direction due to the existence of an image vortex and the lateral velocity of the jet. Figure 5 shows the velocity vector plots of the same $\lambda_j = 1.0$ jet but with a skew angle of $\theta = 45$ deg. A single but stronger vortex is quickly formed. Depending on the jet velocity ratio and the skew angle, this process normally takes place within 2–5 jet diameters downstream of

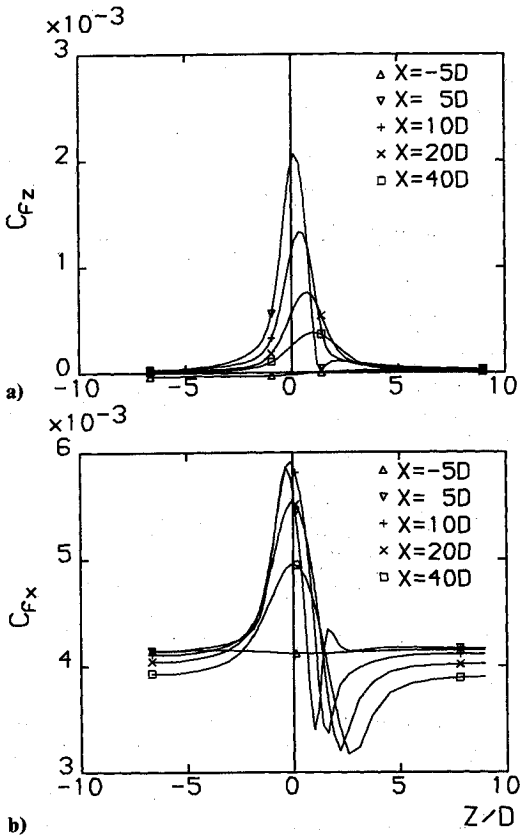

Fig. 7 Stress distribution on the wall produced by a $\theta = 45$-deg jet: a) $C_{fz} = \tau_z/q_e$ and b) $C_{fx} = \tau_x/q_e$.

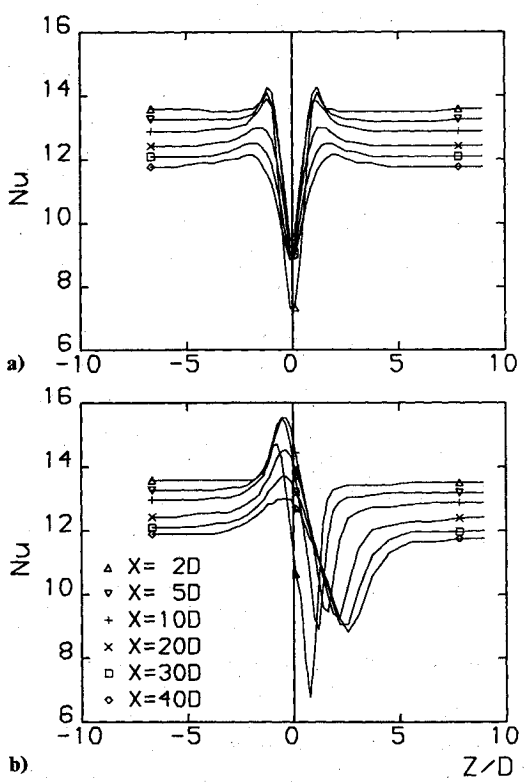

Fig. 8 *Nu* induced by the two $\lambda_j = 1.0$ jets: a) $\theta = 0$ deg and b) $\theta = 45$ deg.

the jet exit. The turbulent kinetic energy distribution, though, still shows the influence of the jet core at a farther downstream plane ($X = 10D$ in Fig. 6). The characteristics of the single vortex become obvious downstream of $X = 20D$. If the jet is properly set up, this single vortex could remain coherent

for a long distance downstream and exercise a favorable influence on the control process. The surface stress distribution certainly demonstrates the characteristics of the single vortex, where Fig. 7a gives the lateral skin friction coefficient distribution reflecting the counter-clockwise motion of the vortex. In Fig. 7b, the high longitudinal skin friction coefficient is brought about by the high kinetic energy fluid swept to the near-wall area by the vortical motion. The low coefficient is the result of the stagnant fluid cumulating at one side of the vortex and this is not swept out of the boundary layer by the vortex (see the next section as well). It is noticeable that although the maximum skin coefficient decreases gradually downstream with the diffusion of the vortex the lowest skin

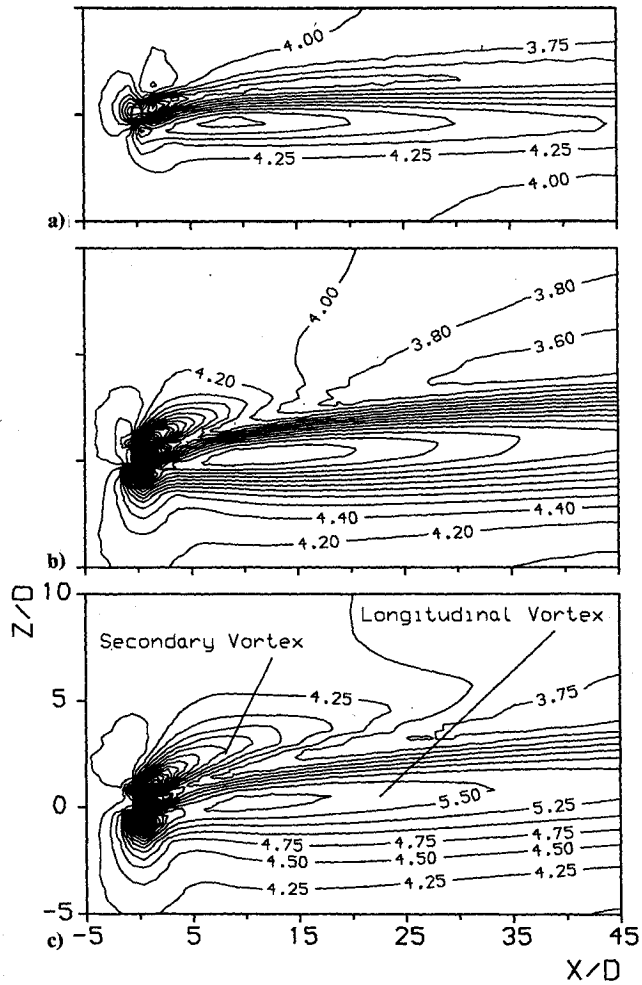

Fig. 9 Longitudinal skin friction coefficient distributions at $\theta = 45$ deg: a) $\lambda_j = 0.7$, b) $\lambda_j = 2.0$, and c) $\lambda_j = 3.0$.

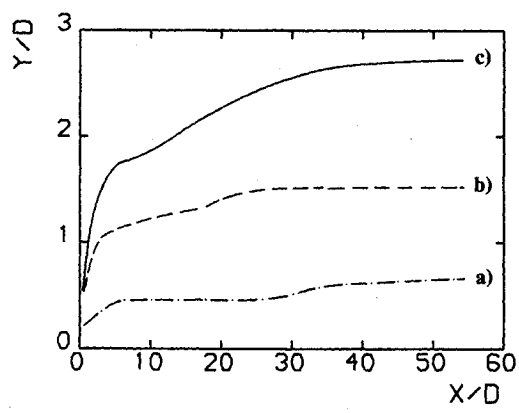

Fig. 10 Jet centerlines at $\theta = 45$ deg: a) $\lambda_j = 0.7$, b) $\lambda_j = 2.0$, and c) $\lambda_j = 3.0$.

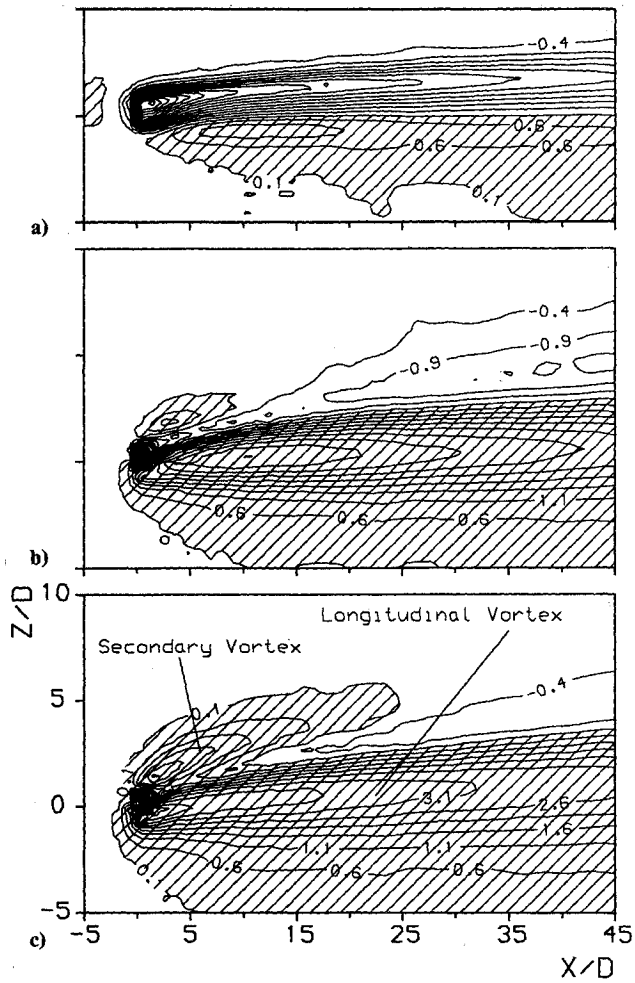

Fig. 11 Relative *Nu* distributions, with the shaded areas indicating value above that of the jet-off situation, at $\theta = 45$ deg: a) $\lambda_j = 0.7$, b) $\lambda_j = 2.0$, and c) $\lambda_j = 3.0$.

friction coefficient remains relatively constant after a few jet diameters downstream. The lateral position of the lowest skin friction coefficient, though, moves with the vortex. So the ability of the vortex to transfer kinetic energy across the boundary layer would diminish downstream and the induced stagnant fluid on one side of the vortex is affected to a less extent by the vortex diffusion. This observation seems a reasonable interpretation for the present study where the vortex remains largely coherent. The implication is significant as this would mean a decrease in the kinetic and thermal energy convection ability and, at the same time, the hot spots (or region) would stay very much the same downstream.

The ability of the longitudinal vortex to transfer the thermal energy is clearly shown in the heat transfer coefficient induced on the wall (Figs. 8a and 8b). Where the high kinetic energy fluid is brought to the wall, the heat transfer coefficient is increased as well. The stagnant fluid accumulated on one side of the vortex introduces hot spots and reduces heat transfer. This observation is, of course, applicable only to a single vortex. In actual applications, it is likely that an array of vortices would be used. These vortices could be designed so areas of stagnant fluid are eliminated.

B. Jet Velocity Ratio

The present study focuses solely on the longitudinal vortices produced by a single jet. Different emphases, though, should be placed when control of flow or the heat transfer are considered. When an array of longitudinal vortices are used for flow control such as separation suppression, the vortex strength does not need to be exceedingly high for the control to be effective. Generally, the likely position of the impending sepa-

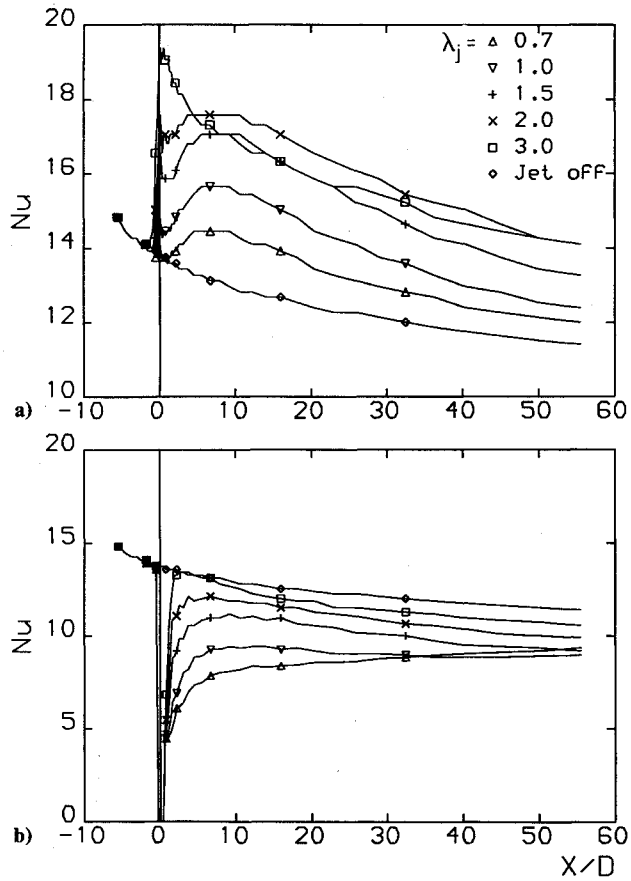

Fig. 12 a) Maximum *Nu* downstream of the jet exit at various jet velocity ratios and b) minimum *Nu*.

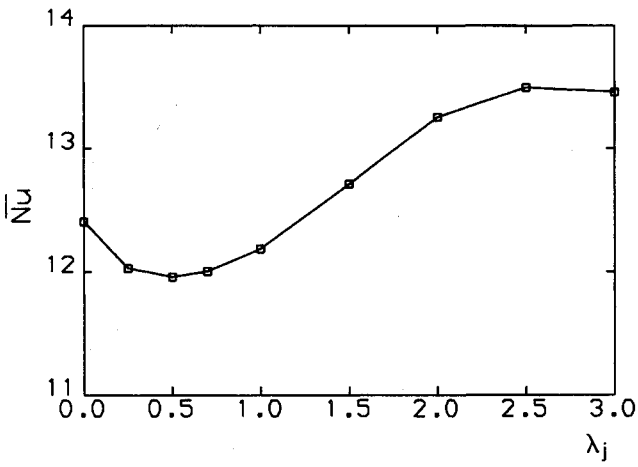

Fig. 13 $\overline{Nu}$ at various jet velocity ratios indicating three types of vortex production.

ration is known. The vortices could be generated just ahead of the separation to suppress it. The winglet and the jet could then be designed accordingly to minimize the drag and pressure loss. If the vortices are used to enhance heat transfer, the objective is different. An area of high heat transfer coefficient has to be produced on the control surface. Areas of low heat transfer coefficient should be kept as small as possible. This, however, is not so critical when we only consider a single jet for the reason discussed in the last part of Sec. IV.A. The differences should be born in mind when discussing the effects of jet velocity and skew angle.

When the oncoming flow remains the same as in the present case, changes in the jet velocity ratio mean variations in the jet momentum efflux. This would alter the initial vorticity production at the jet exit, the position of the vortex (defined by the maximum vorticity in this study), and the strength of the vortex. The stress distribution on the wall is closely connected to the relative position and strength of the vortex. The relationship between the vortex and the desired heat transfer enhancement is, however, not necessarily straightforward. Depending on the position and diffusion process, there are three types of vortex. If the jet velocity is too low, the longitudinal vortex could be deeply embedded in the boundary layer where the turbulent diffusion is significant. The vortex (or vortices) produced will then be diffused fairly rapidly. Thus, the favorable effect of the vortex on the heat transfer enhancement is limited. In the meantime, the stagnant fluid accumulated on one side of the vortex will cause hot spots on the wall. If the jet velocity is too high, the jet could penetrate the boundary layer resulting in the formation of a vortex outside the layer. Although the vortex could be strong and remain coherent for a long distance, the effectiveness is likely to be reduced and it is clearly not cost effective. To achieve the desirable flow and heat transfer control, the jet needs to be set up at an optimal velocity and skew and pitch angles to generate a coherent and properly positioned vortex.

The three types of vortex productions are shown in Figs. 9a–9c through skin friction coefficient on the wall. On one side of the jet, an area of high longitudinal skin friction due to the longitudinal vortex dominates. At high jet velocity ratios such as $\lambda_j = 2.0$ and 3.0, there is another area of high skin friction, which is due to the secondary vortex: the weak vortex produced by the initial vorticity production at the jet exit. In between these two areas of high skin friction, the stagnant fluid which is not swept away from the boundary layer induces an area of low skin friction. Figure 9a is due to a $\lambda_j = 0.7$ jet.

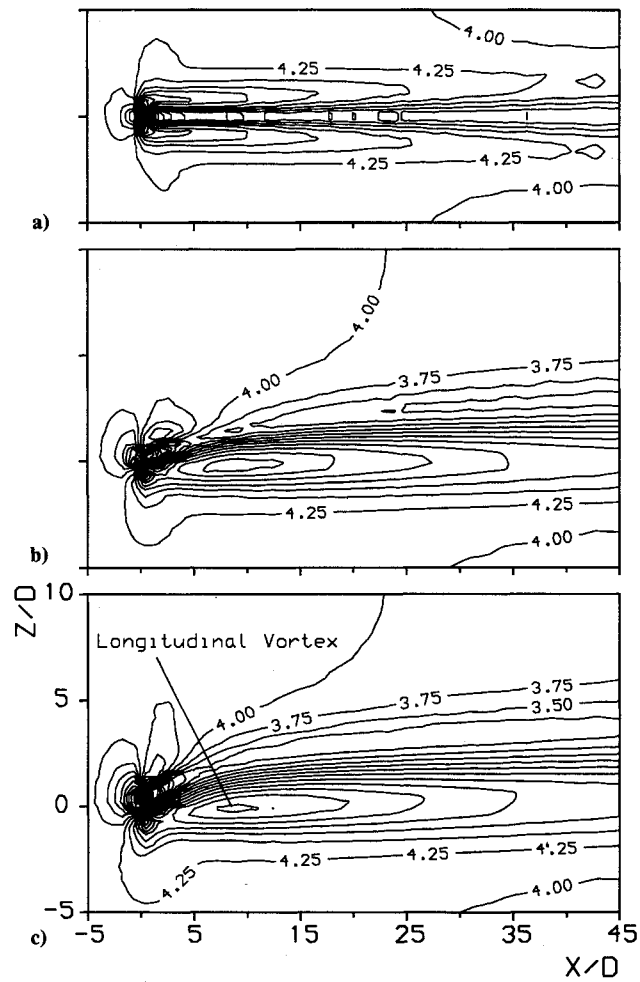

Fig. 14 Longitudinal skin friction coefficient distributions at $\lambda_j = 1.0$: a) $\theta = 0$ deg, b) $\theta = 45$ deg, and c) $\theta = 90$ deg.

In this case, the longitudinal vortex is rather weak, thus the limited high skin friction coefficient area on one side of the vortex. The effect of the secondary vortex is not significant. Figure 9b indicates a larger area of high skin friction coefficient induced by the $\lambda_j = 2.0$ jet. The low skin friction area is reduced. Also, the area of relatively high skin friction coefficient on the other side of the vortex, which is the result of initial vorticity production, becomes much larger and clearer. This type of stress distribution is produced by the $\lambda_j = 3.0$ jet as well. However, the maximum skin friction coefficient is not necessarily increased (Fig. 9c). Obviously, the ideal heat transfer result would be achieved using the stress distribution in Fig. 9b.

The point made about the effectiveness of the vortex is further demonstrated by the vortex centers from the wall (Fig. 10). In the present study, the oncoming boundary layer has a thickness of 2.2*D*. The $\lambda_j = 0.7$ jet is seen deeply embedded in the boundary layer and subsequently diffused rapidly. The $\lambda_j = 2.0$ jet seems to have produced a longitudinal vortex sitting at the outer region of the boundary layer. This type of longitudinal vortex is desirable as a balance is achieved between the vortex diffusion and its effectiveness in the mass and thermal convection. The $\lambda_j = 3.0$ jet results in a vortex outside the boundary layer. It will be shown later that, although the velocity ratio is increased, the effectiveness is reduced by the increased distance away from the wall.

The impact of the three types of vortex on heat transfer is shown by Figs. 11a–11c. The Nusselt number given is the difference between the jet-on and jet-off conditions. The increase in the Nusselt number above that of a jet-off condition is indicated by the shaded areas. The $\lambda_j = 0.7$ jet produces a small increase in the heat transfer coefficient in the high stress area but a significant reduction in the low stress area. (Heat transfer coefficient will be referred to wherever possible instead of Nusselt number.) The low heat transfer coefficient

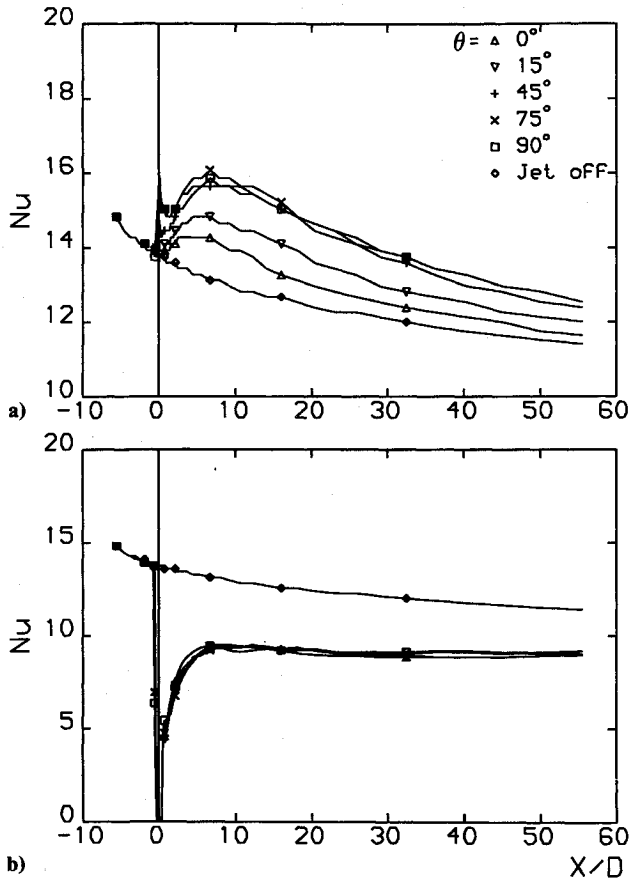

Fig. 16 a) Maximum *Nu* tracked downstream of the $\lambda_j = 1.0$ jet exit and b) minimum *Nu*.

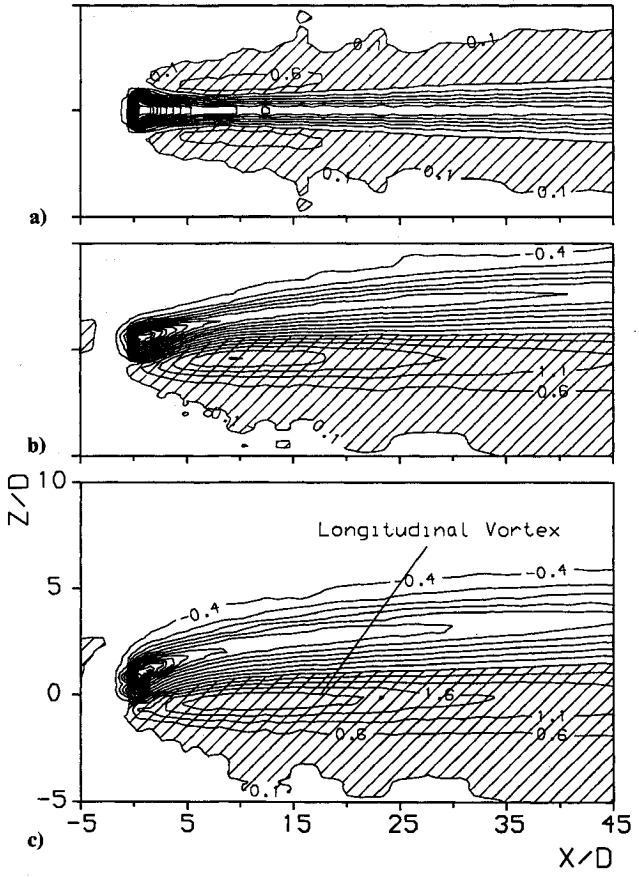

Fig. 15 Relative *Nu*, with the shaded areas indicating value above that of the jet-off situation, at $\lambda_j = 1.0$: a) $\theta = 0$ deg, b) $\theta = 45$ deg, and c) $\theta = 90$ deg.

area is quite pronounced in this case. It seems that the hot spots exist over a large area downstream of the jet exit. This type of flow has an adverse effect on the convective heat transfer. The $\lambda_j = 2.0$ and 3.0 jets, on the other hand, induce areas of high heat transfer coefficient, and the areas with low heat transfer coefficient are reduced compared to that due to the $\lambda_j = 0.7$ jet. The high heat transfer coefficient distribution covers large areas and lasts well downstream. Apart from the area of high heat transfer coefficient due to the main vortex, the secondary vortex also induces high heat transfer coefficient. This type of distribution indicates heat transfer enhancement. Figure 11c, though, does not show a substantial increase in the heat transfer ability over the $\lambda_j = 2.0$ jet. In fact, the maximum Nusselt number (Fig. 12a) tracked downstream of the jet exit suggests that the increase in the heat transfer coefficient is marginal when $\lambda_j \geq 1.5$. This observation is further confirmed by $\overline{Nu}$ in Fig. 13. $\overline{Nu}$ of the jet-off condition is 12.4. As the jet is switched on, $\overline{Nu}$ drops below the jet-off value, and then gradually rises above it as the jet velocity ratio increases. There are three jet velocity ratio ranges of interest. The first lies between $0.0 < \lambda_j < 1.2$. In this range, the vortex is not strong enough to remain coherent for a suitable distance. As the jet is weak, the vortex lies deep within the boundary layer. Its ability to convect kinetic and thermal energy across the boundary layer is severely restricted. In the meantime, the accumulated stagnant fluid on one side of the vortex induces hot spots on the wall, thus reducing the heat transfer. In the second range ($1.2 < \lambda_j \leq 2.5$), $\overline{Nu}$ rises considerably with the jet velocity ratio and reaches a maximum at $\lambda_j = 2.5$. As λ_j increases, the vorticity is increased as well. The location of the vortex now lies in the outer region of the layer. The result points to an improved ability of mass and thermal convection across the boundary layer. As the vortex is comparatively strong, the stagnant fluid is swept away from the boundary layer more effectively. Those factors combine to

enhance the heat transfer. The third range lies above $\lambda_j \geq 2.5$. Here, the jet has effectively penetrated the boundary layer and the longitudinal vortex now lies outside the layer. Although the vorticity could remain coherent, the ability for mass and thermal convection is reduced due to the larger distance away from the wall.

C. Jet Skew Angle

If the momentum efflux and pitch angle are kept constant, changes in the skew angle would alter not only the jet path by introducing a lateral velocity component but also the initial vorticity production around the jet exit. A single vortex is eventually formed (see Sec. IV.A). This will have implications in the mass and thermal convection across the boundary layer.

The longitudinal skin friction coefficient (Figs. 14a–14c) shows that the high stress area on the wall due to the vortex is increased as the jet skew angle is increased. The maximum skin friction coefficient tracked downstream of the jet indicates a rapid rise between $0 < \theta \leq 45$ deg and only a slight change above 45 deg. This observation is in broad agreement with that noted by Compton and Johnston.[5] The minimum skin friction, on the other hand, shows little variation over the skew angle range studied. It implies that the ability of the vortex to sweep the stagnant fluid out of the boundary layer does not depend on the jet skew angle. It is also worth noting here that the jet position relative to the wall does not change with the skew angle. Apart from the preceding observations, the secondary flow features due to the weak vortex disappear with the skew angle increase.

The heat transfer coefficient is given in Figs. 15a–15c in terms of Nusselt number. Again, the value given is the difference between the jet-on and the jet-off conditions. Between $\theta = 45$ and 90 deg, the area of high heat transfer coefficient remains basically the same with only a slight increase in the maximum value. The area of low heat transfer coefficient also experiences only small variations. This correlates with the characteristics of the longitudinal stress distribution on the wall and reflects the various aspects of behavior of the vortex.

The effects of the jet skew angle are clearly illustrated in Fig. 16 (only selected skew angles are given) through the maximum and minimum Nusselt number tracked downstream of the jet exit. The minimum Nusselt number does not vary with the skew angle. A significant increase in the maximum Nusselt number is observed between $0 < \theta \leq 45$ deg. This indicates increased vorticity and circulation levels in the boundary layer. For $\theta > 45$ deg though, there is no significant variation. This observation does not imply that no benefit can be extracted from the larger skew angle as the area of influence may vary. This somewhat subtle feature is not addressed in this study.

V. Concluding Remarks

The present study sets out to investigate the fluid flow and thermal fields induced by small pitched and skewed jets at various velocity ratios. As the vorticity field changes substantially with the jet velocity ratio and the skew angle, the induced stress and thermal fields on the wall vary as well, with different implications in the control process.

The longitudinal vortex is found to induce an area of high longitudinal skin friction and heat transfer coefficient on one side of the jet. On the other side of the jet, a secondary vortex is observed under certain ranges of jet velocity ratio and skew angle. It also induces an area of high longitudinal skin friction and heat transfer coefficient. The effects of the secondary vortex increase with the jet velocity ratio but decrease with the jet skew angle. The longitudinal vortex also produces stagnant fluid accumulating on one side of the longitudinal vortex, which is not swept out of the boundary layer by the vortical motion, and results in an area of low longitudinal skin friction and heat transfer coefficient.

Changes in the jet velocity ratio give rise to three types of vorticity distribution. The first corresponds to a weak longitudinal vortex ($0 < \lambda_j \leq 1.2$ under the present flow condition). The jet is deeply embedded in the turbulent boundary layer. The vortex is diffused rapidly through turbulent mixing and does not remain coherent over a long enough distance downstream. This type of vortex may be useful for flow control but actually reduces the heat transfer. The second type corresponds to a longitudinal vortex positioned at the edge or in the outer region of the boundary layer. Here, a balance is achieved between the vortex diffusion and its ability for mass and thermal convection. The vortex remains coherent for a suitable distance downstream. The jet velocity range for this type of vortex is $1.2 < \lambda_j \leq 2.5$. Within this range, the maximum skin friction coefficient and heat transfer coefficient increase rapidly. At the same time, the minimum skin friction coefficient and heat transfer coefficient approach that of the jet-off values. The third type corresponds to a longitudinal vortex positioned outside of the turbulent boundary layer. The jet has now penetrated the layer. Although the longitudinal vortex may be stronger and remains coherent, the improvements in the skin friction coefficient and heat transfer coefficient are marginal.

There are only small variations in the skin friction and heat transfer characteristics when the jet skew angle is above 45 deg. Between $0 < \theta \leq 45$ deg, the maximum skin friction coefficient and heat transfer coefficient will increase with the skew angle. The minimum skin friction coefficient and heat transfer coefficient, though, experience little change for the range of the skew angle studied.

Acknowledgment

We wish to thank H. H. Pearcey and F. S. Henry for their comments during the course of the study.

References

[1]Pearcey, H. H., "Shock Induced Separation and its Prevention by Design and Boundary Layer Control," *Boundary Layer and Flow Control,* Vol. 2, edited by G. V. Lachman, Pergamon, New York, 1961, pp. 1170–1344.

[2]Adkins, R. C., "Diffusers and Their Performance, Improvement by Means of Boundary Layer Control," AGARD-R-654, No. 6, June 1977.

[3]Wallis, R. A., "The Use of Air Jets for Boundary Layer Control," Aerodynamics Research Lab., Aero Note 110 (N-34736), Melbourne, Australia, Jan. 1952.

[4]Johnston, J. P., and Nishi, M., "Vortex Generator Jets—Means for Flow Separation Control," *AIAA Journal,* Vol. 28, No. 6, 1990, pp. 989–994.

[5]Compton, D. A., and Johnston, J. P., "Streamwise Vortex Production by Pitched and Skewed Jets in a Turbulent Boundary Layer," *AIAA Journal,* Vol. 30, No. 3, 1992, pp. 640–647.

[6]Freestone, M. M., "Preliminary Tests at Low Speeds on the Vorticity Produced by Air-Jet Vortex Generators," Dept. of Aeronautics, City Univ., Research Memo Aero 85/01, London, England, UK, Feb. 1985.

[7]Honami, S., Shizawa, T., Uchiyama, A., and Yamamoto, M., "An Experimental Study of Film Cooling in the Lateral Injection," *Proceedings of the 1991 Yokohama International Gas and Turbine Congress* (Yokohama, Japan), Oct.–Nov. 1991, pp. 207–214.

[8]Zhang, X., "Interaction between a Turbulent Boundary Layer and Elliptic and Rectangular Jets," *Proceedings of the 2nd International Symposium on Engineering Turbulence Modeling and Measurements* (Florence, Italy), Elsevier, May–June 1993, pp. 251–260.

[9]Edwards, F. J., and Alker, C. J. R., "The Improvement of Forced Surface Heat Transfer Using Surface Protrusions in the Form of (A) Cubes and (B) Vortex Generators," *Proceedings of the 5th International Heat Transfer Conference* (Tokyo, Japan), Vol. 2, 1974, pp. 244–248.

[10]Russell, C. M. B., Jones, T. V., and Lee, G. H., "Heat Transfer Enhancement using Vortex Generators," *Proceedings of the 7th International Heat Transfer Conference* (Munich, Germany), Vol. 3, 1982, pp. 283–288.

[11]Fiebig, M., Kallweit, P., Mitra, N. K., and Tiggelbeck, S., "Heat Transfer Enhancement and Drag by Longitudinal Vortex Generators in Channel Flow," *Experimental Thermal and Fluid Science,* Vol. 4, No. 1, Jan. 1991, pp. 103–114.

[12]Fiebig, M., Brockmeier, U., Mitra, N. K., and Guntermann, T.,

"Structure of Velocity and Temperature Fields in Laminar Channel Flows with Longitudinal Vortex Generators," *Numerical Heat Transfer,* Part A, Vol. 15, April 1989, pp. 281–302.

[13]Eibeck, P. A., and Eaton, J. K., "The Effects of Longitudinal Vortices Embedded in a Turbulent Boundary Layer on Momentum and Thermal Transport," *Proceedings of the 8th International Heat Transfer Conference* (San Francisco, CA), Vol. 3, 1986, pp. 1115–1120.

[14]Launder, B. E., and Spalding, D. B., "The Numerical Computation of Turbulent Flows," *Computational Methods in Applied Mechanical Engineering,* Vol. 3, No. 2, May 1974, pp. 269–289.

[15]Zhang, X., "Computational Analysis of Co- and Contra-Rotating Longitudinal Vortices in a Turbulent Boundary Layer," AIAA Paper 93-3035, July 1993.

[16]Shizawa, T., and Eaton, J. K., "Turbulent Measurements for a Longitudinal Vortex Interacting with a Three-Dimensional Turbulent Boundary Layer," *AIAA Journal,* Vol. 30, No. 1, 1992, pp. 49–55.

[17]Rhie, C. M., and Chow, W. L., "Numerical Study of the Turbulent Flow past an Airfoil with Trailing Edge Separation," *AIAA Journal,* Vol. 21, No. 11, 1983, pp. 1527–1532.

[18]Van Doormaal, J. P., and Raithby, G. D., "Enhancement of the SIMPLE Method for Predicting Incompressible Fluid Flows," *Numerical Heat Transfer,* Vol. 7, April–June 1984, pp. 147–163.

[19]Chen, C. L. H., "Aufrollung Eines Zylindrischen Strahles Durch Querwind," Ph.D. Dissertation, Univ. of Gottingen, Germany, 1942.

[20]Ing, D., "A Study of the Mean Flow Structure of Circular and Rectangle Exit Turbulent Jets Initially at a Small Incidence Angle to a Uniform Mainstream," Ph.D. Dissertation, Univ. of Southampton, Southampton, U.K., 1981.